Surface albedo as a proxy for land-cover change in seasonal dry forests: evidence from the Brazilian Caatinga biome

John Cunha[a, e, *], Rodolfo L. B. Nóbrega[b] , Iana Rufino[a], Stefan Erasmi[c], Carlos Galvao[a,d], Fernanda Valente[e]

[a]Federal University of Campina Grande, Center for Natural Resources and Technology, Campina Grande, Brazil;
[b]University of Reading, School of Archaeology, Geography and Environmental Science, Reading, United Kingdom;
[c]University of Gottingen, Institute of Geography, Cartography GIS & Remote Sensing Section, Goettingen, Germany;
[d]Griffith University, Cities Research Institute, Nathan Campus, Queensland 4111, Australia;
[e]University of Lisbon, School of Agriculture, Forest Research Centre (CEF), Tapada da Ajuda, 1349-017 Lisbon, Portugal.
*Corresponding author: john.brito@ufcg.edu.br

Abstract:

Ongoing increases in human and climate pressures associated with the lack of monitoring initiatives make the Caatinga one of the most vulnerable biomes in the world. The Caatinga is located in the semi-arid region of Brazil, and its vegetation phenology is highly dependent on precipitation, which has a high spatial and temporal variability. Under these circumstances, satellite image-based methods are valued due to their ability to uncover human induced changes from climate effects on land cover. In this study, 670 continuous Landsat images over a period of 31 years (1985–2015) were analysed to investigate spatial and temporal patterns of land-cover change (LCC) due to vegetation clearing in an area of the Caatinga biome. We compared the performance of surface albedo (SA), the Enhanced Vegetation Index (EVI) and the Normalized Difference Vegetation Index (NDVI) to evaluate their suitability for monitoring LCC driven by human actions in contrast to precipitation-related variations. We applied a residual trend analysis, with detection of significant breakpoints (TSS-RESTREND), to a monthly Landsat time series. Our results show that SA was able to identify the year of land-cover clearing with a higher accuracy (83%) than that of EVI (20%) and NDVI (34%). The overall outcome of the study shows the benefits of using

different spectral bands instead of greenness indices of Landsat time series for the monitoring of LCC, as a result of environmental land surface processes in seasonal dry forests such as the Caatinga.

Keywords: Dryland degradation; vegetation index; land-cover clearing; seasonal dry forest; semi-arid climate

1 Introduction

Distinguished land cover alteration, driven by natural climatic variability or by human action, is one of the main challenges when studying seasonal dry forests (Yang et al., 2016; Wessels et al., 2007). In these areas, greenness is strongly related to the annual precipitation averages as well as the spatial variability and shifts of the rainy season period within a year (Hein et al., 2011). Impacts caused by human actions in seasonal dry forests are often masked by intra-annual climatic variability, especially after long drought periods (Wessels et al., 2007; Zhang et al., 2014). The Caatinga is a biome that has both of these characteristics. Located in northeastern Brazil, in a semi-arid region with high temporal and spatial rainfall variability (Andrade-Silva et al., 2012), the Caatinga vegetation is a heterogeneous (Rodal et al., 2008), seasonal semi-deciduous dry forest (Brito et al., 2012; Albuquerque et al., 2012), with its phenology driven by short-term rainfall patterns (Erasmi et al., 2014; Lima and Rodal, 2010). In addition to these biophysical characteristics, the land cover change (LCC) in the Caatinga is strongly shaped by the human way of using and living on the land (Andrade-Silva et al., 2012; Araújo et al., 2007, 2010; Santos and Tabarelli, 2002). Unlike most seasonal dry tropical forests that occur in isolated spots, the Caatinga biome spreads over a vast contiguous area, occupying ca. 830,000 km^2 (CNUC, 2017; Linares-Palomino et al., 2011). Although it is a unique ecosystem with a high degree of biodiversity and number of endemic species (Sobrinho et al., 2016), only 7.7% of its area is under environmental protection by the Brazilian National System of Units of Conservation

(1.3% of restricted protection areas plus 6.4% of sustainable use areas) (CNUC, 2017). The Caatinga is considered the most neglected and threatened Brazilian biome due to inadequate and unsustainable use of its natural resources over the past decades (Moro et al., 2016). Native vegetated areas of this biome have been gradually replaced by crops and pastures for livestock or urban areas (Leal et al., 2005; Santos et al., 2012). According to Sobrinho et al. (2016), slash-and-burn agriculture, cattle ranching, vegetation management for fuelwood and short fallow periods are transforming Caatinga into a complex mosaic of agricultural, pasture and small forest patches.

Orbital remote sensing data are a source of information for the monitoring of vegetation dynamics (Schucknecht et al., 2013). Most vegetation studies that analyse long (> 30-years) remote sensing time series use vegetation indices in low spatial resolution (i.e., 1 to 8 km) (Leroux et al., 2017). However, in many cases, this resolution is not sufficient to detect anthropogenic impacts on land cover. The local nature of human actions on the land can only be seen in an analysis using refined spatial resolutions (Lambin et al., 2003; Stroppiana et al., 2012). Landsat datasets are one of the most valuable sources of global observation, owing to more than 30 years of multispectral data, i.e., visible, near, medium and thermal infrared ranges, which constitute the longest continuous remotely sensed record of the Earth's surface (Loveland and Dwyer, 2012). Landsat imagery quality has been improved in recent years. The new data structure provides information on radiometric, geometric and cloud cover quality to support temporal analysis (Wulder et al., 2016). Such improved higher-level products were recently made freely available by the USGS and allow users to access surface reflectance data (Ju and Masek, 2016). Landsat data can provide vegetation indices as well as other variables that use different ranges of the electromagnetic spectrum, such as the broadband surface albedo (0.3–3 μm). Surface albedo (SA) can be an accurate indicator of LCC because it is sensitive to seasonal phenological variations (Wang et al., 2017) and changes in soil properties caused by human management practices

(Cai et al., 2016; Shuai et al., 2011; Wang et al., 2016). Despite the recognized ability of the SA to show LCC, it has not been used to distinguish between the effects of climate variability and anthropogenic alteration in seasonal dry forests (Karlson and Ostwald, 2016; Leroux et al., 2017).

Different approaches based on orbital data have been used to distinguish between the effects of climatic and anthropogenic variability on land cover in seasonal dry forests (Anyamba et al., 2014; DeVries et al., 2015; Evans and Geerken, 2004; Higginbottom and Symeonakis, 2014; Ibrahim et al., 2015; Karlson and Ostwald, 2016; Leroux et al., 2017; Verbesselt et al., 2016). In most of these studies, changes in the environment are identified by time series trend techniques. In this sense, two methods are highlighted due to their effectiveness in seasonal dry forests: the Break detection For Additive Season and Trend (BFAST, DeVries et al., 2015; Dutrieux et al., 2015; Verbesselt et al., 2012) and the RESidual TREND (RESTREND, Evans and Geerken, 2004; Li et al., 2016; Wessels et al., 2012) methods. Dutrieux et al. (2015) showed a significant improvement in the identification of LCC (breakpoints) in BFAST when they used external regressors, which removed seasonal climatic effects. Indeed, breakpoints in a time series can be a result of climatic effects on the analysed variable, such as the effects of rainfall on the Normalized Difference Vegetation Index (NDVI) (Jong et al., 2012). Despite RESTREND being a well-known method with a solid theoretical background, this method requires more sensitive analytical procedures, capable of coping with inter-annual rainfall variability and trends for detection of realistic levels of human-induced land degradation (Wessels et al., 2012).

The Time Series Segmentation and RESidual TREND method (TSS-RESTREND, Burrell et al., 2017) was recently developed to overcome limitations identified in both BFAST and RESTREND techniques and takes into account seasonal climate effects and identification and removal of breakpoints due to rainfall variability. TSS-RESTREND uses the procedure of breakpoint identification of the BFAST associated with the RESTREND seasonal climate effects filter and adds the Chow test (Chow, 1960), to consider the breakpoint with the highest significance in the time series for each pixel. By incorporating relevant mechanisms and reducing the limitations identified in the BFAST and RESTREND, the TSS-RESTREND indicates a high potential to be applied in a land cover clearing analysis in seasonal dry forests.

In this study, we applied the TSS-RESTREND technique to a 31-year Landsat time series and compared its results with field observations from an area of the Caatinga. Our hypothesis was that the SA is a better indicator for LCC detection in the Caatinga than are other greenness indices such as EVI and NDVI. This paper has two objectives: 1) to use long-term spectral Landsat data to validate the TSS-RESTREND method in identifying LCC in a seasonal dry forest area; and 2) to assess the performance of SA in identifying LCC compared to that of other proxies for vegetation condition, i.e., EVI and NDVI.

2 Study area and data

2.1 Study area

The study area is located in the Caatinga biome, northeastern Brazil (Fig. 1A). Livestock is one of the main economic activities in this region (Belchior at al., 2017), leading to substantial LCC (Fig. 1B and C). The climate is hot semi-arid (BSh, Köppen classification) (Alvares et al., 2013), with only two distinct seasons: the very hot rainy season (from February to May) and the hot dry season (from June to January). The average annual rainfall in this region is approximately 550 mm, with high interannual variability (coefficient of variation of approximately 30%) and an average annual temperature of 23°C. Figure 2 shows the Standard Precipitation-Evapotranspiration Index (SPEI) for 12 months (Vicente-Serrano et al., 2010) and the precipitation for the studied period and area. As can be observed, the region presents alternation between dry and wet periods of different intensities.

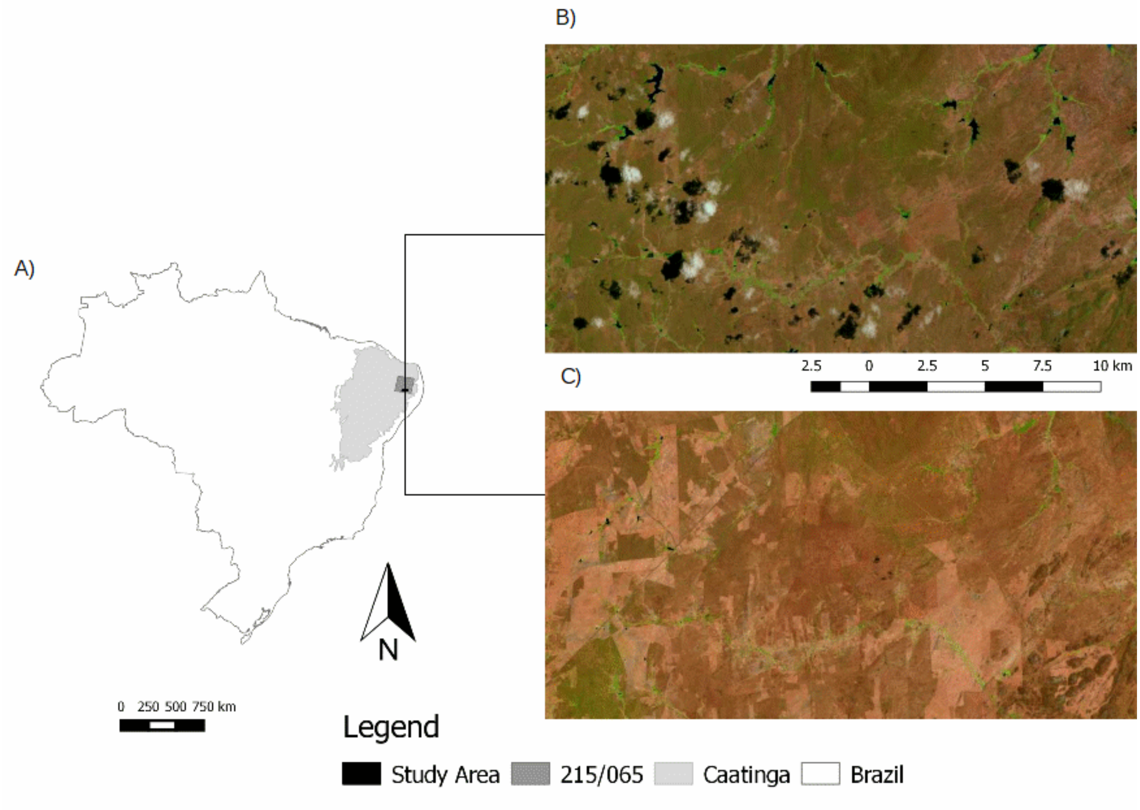

Fig. 1 - (A) Location of the Brazilian semi-arid region, Landsat scene 215/065 (path/row) and study area (Xmin: -37.07; Xmax: -36.84; Ymin: -7.86; Ymax: -7.74, WGS 84); (B) Landsat images of the study area on 10/07/1984; (C) the same area on 09/27/2015, showing land-cover differences between the first and last years of the analysed period

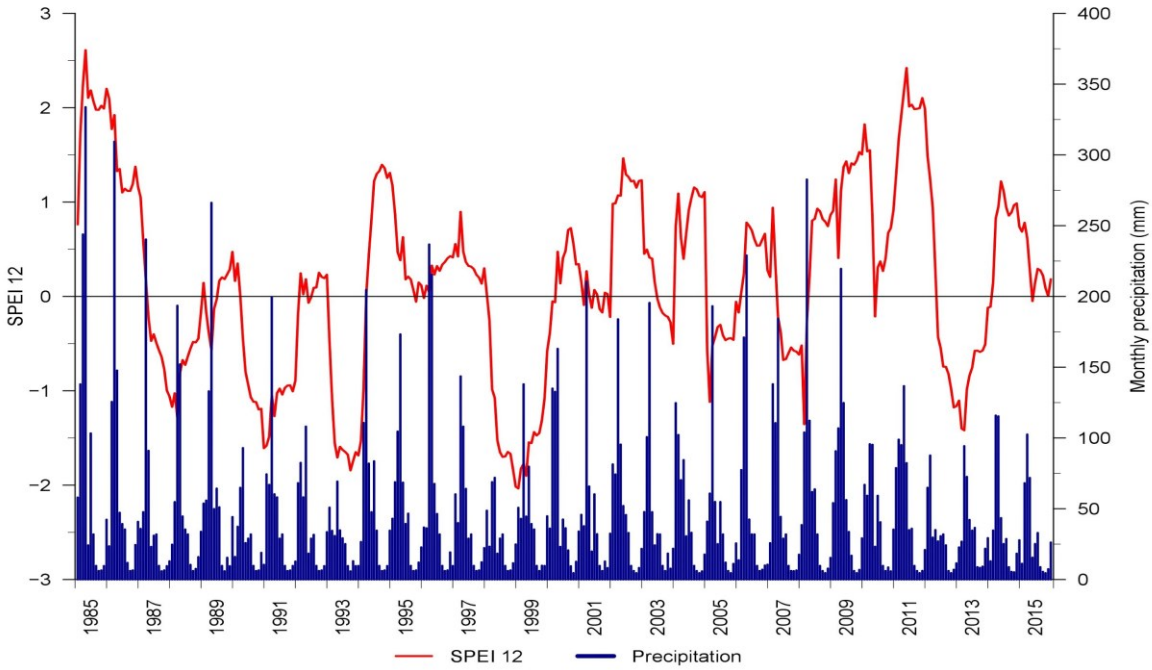

Fig. 2 - The 12-month Standardized Precipitation-Evapotranspiration Index - SPEI 12 (Beguería et al., 2017) and CHIRPS Precipitation (Funk et al., 2015) at geographic coordinates x: -36.75, y: -7.75, WGS 84.

2.2 Datasets

2.2.1 Landsat Surface Reflectance

In this study, we used the atmospherically corrected surface reflectance (SR), one of the products processed from the raw data collected by the sensors on-board the Landsat satellites and made freely available by the United States Geological Survey. Standard processing of SR is performed by USGS, including the Level 1 Standard Terrain Correction, resulting in ortho-rectified images of high geometric accuracy. SR data are generated by two different algorithms, depending on the measuring sensor: Landsat 5 TM and 7 ETM+ SR data are obtained by the LEDAPS software (Masek et al., 2006), whereas Landsat 8 OLI data are processed by the LaSRC algorithm (Vermote et al., 2016).

We identified 670 available Landsat images that cover the study period (1985–2015) (390 by TM sensor, 233 by ETM+ and 47 by OLI). We used the Landsat Surface Reflectance Quality Assessment (pixel_qa) to guarantee the quality of the analysis. Only pixels classified as “clear” (values 66 and 130 on Landsat 5 and 7 files or 322 and 386 on Landsat 8) were considered as good quality observations and used in our analyses.

2.2.2 RapidEye

RapidEye images cover the Earth's surface since 2009 and are available in tiles of 25 × 25 km^2 with 5 m of spatial resolution and 5 spectral bands. In this work, we used two tiles (2435424 and 2435524) from datasets of the period 2012 to 2015, which were made freely available by the Brazilian Ministry of the Environment (MMA, 2018) for academic use.

2.2.3 Precipitation

The precipitation data used in this work were obtained from the Climate Hazards group InfraRed Precipitation with Stations (CHIRPS) dataset (Funk et al., 2015; Katsanos et al., 2016). CHIRPS is a near-global, very high spatial resolution (0.05° grid) precipitation product developed for monitoring environmental changes over land (Funk et al., 2015). We used monthly precipitation data from October 1983 to December 2015.

3 Methods

3.1 Spectral variables

The identification of LCC was applied by using the NDVI (Tucker, 1979), the EVI (Huete et al., 2002, 1997) and the surface albedo (SA) (Shuai et al., 2014; Wang et al., 2016). For each Landsat image, NDVI, EVI and SA were calculated using Eqs. (1) to (3).

$$NDVI = \frac{\rho_{NIR} - \rho_{red}}{\rho_{NIR} + \rho_{red}} \quad (1)$$

$$EVI = 2.5 \times \frac{\rho_{NIR} - \rho_{red}}{\rho_{NIR} + 6 \times \rho_{red} - 7.5 \times \rho_{blue} + 1} \quad (2)$$

$$SA = b_{blue} \times \rho_{blue} + b_{green} \times \rho_{green} + b_{red} \times \rho_{red} + b_{NIR} \times \rho_{NIR} + b_{SWIR1} \times \rho_{SWIR1} + b_{SWIR2} \times \rho_{SWIR2} + b_0 \quad (3)$$

where ρ and b are the surface bidirectional reflectance values and their corresponding conversion coefficients for the six non-thermal Landsat bands, i.e., blue, green, red, near-infrared (NIR) and the two shortwave infrared (SWIR1 and SWIR2) bands. Table 1 presents the b values of several spectral bands of the three satellites used in this study.

Table 1 - Band conversion coefficients used to calculate shortwave albedo for the different Landsat data.

Sensor	b_{blue}	b_{green}	b_{red}	b_{NIR}	b_{SWIR1}	b_{SWIR2}	b_0
Landsat-5 TM	0.3206	0	0.1572	0.3666	0.1162	0.0457	- 0.0063
Landsat-7 ETM+	0.3141	0	0.1607	0.3694	0.1160	0.0456	- 0.0057
Landsat-8 OLI	0.2453	0.0508	0.1804	0.3081	0.1332	0.0521	0.0011

The highest values of the vegetation indices are found in vegetated areas, while their lowest values occur in areas of bare soil. As surface albedo has an inverse behaviour to vegetation indices, we used the inverse surface albedo (ISA) in the simulations (ISA = 1 - SA).

For analysis that involves a single moment of observation, the presence of cloud and cloud shadow in many pixels may make it partially or totally impossible to visualize the study area. To overcome this problem, Holben (1986) presented a technique for the temporal composition of information coming from orbital sensors. This method is usually called the Maximum NDVI Composite, as the seasonal composite image is created using the highest NDVI value for each pixel in each period (Flood, 2013). Although this technique was initially used only for NDVI with imagery of the Advanced Very High Resolution Radiometer (AVHRR) sensor, it has been successfully applied to other orbital sensors and indices (e.g., Huete et al., 2002). Flood (2013) has showed that the medoid (a multi-dimensional analogue of the median) is a better measure to produce representative temporal image composites. Based on these results, we reduced the initial time-series of the ISA, EVI and NDVI to monthly composite images and calculated the median of each variable in each pixel. The missing values on the monthly time-series of some pixels were gap-filled by linear interpolation. A linear Savitzky–Golay filter was applied (Chen et al., 2004; Savitzky and Golay, 1964), with a five-month half-width smoothing window, in order to reduce the noise caused by cloud contamination and atmospheric variability. This filter was applied to each index (ISA, EVI and NDVI) of monthly time-series in all pixels of the study area.

3.2 TSS-RESTREND

The Time Series Segmentation and RESidual TREND method (TSS-RESTREND), proposed by Burrell et al. (2017), combines the RESidual TREND (RESTREND) technique (Evans and Geerken, 2004) and the Breaks For Additive Seasonal and Trend (BFAST) methodology (Verbesselt et al., 2012, 2010), allowing a better and more accurate detection of structural changes in the ecosystems. Trend analysis is a technique commonly applied in different scientific areas to study the average range of change of some variable along time or space (e.g., Alley, 1988; Lindquist, 2004). However, prior to the application of trend analysis, it is frequently necessary to remove the influence of an exogenous variable, either by parametric (e.g., regression) or nonparametric (e.g., LOWESS) methods, to reduce the variability of the studied variable (Helsel and Hirsch, 2002; Schertz et al., 1991). In remote sensing, a similar procedure has been applied for land-cover analyses. The RESTREND method analyses the temporal trends in vegetation precipitation relationship (VPR) residuals of a linear regression of the NDVI on the precipitation accumulated over some time period (Evans and Geerken, 2004). In Burrell et al. (2017), VPR is obtained for two sets of information: complete time series (CTS) and annual maximum NDVI. In both cases, linear regression is performed with the Optimal Precipitation Accumulated (OPA), which is calculated on a per-pixel basis by an exhaustive search algorithm that combines different accumulation periods and lag times. The pair leading to the highest correlation coefficients between CTS NDVI and annual maximum NDVI is used to establish the optimum VPR.

The TSS-RESTREND method uses annual VPR to exclude pixels that do not meet established criteria to use the RESTREND method (Li et al., 2016; Wessels et al., 2012) and applies BFAST to CTS VPR residuals for the remaining pixels. The application of the BFAST method (Verbesselt et al., 2010) returns a list of potential breakpoints that will be analysed later by the Chow test (Chow, 1960) to determine if there is a significant breakpoint. After identifying a significant breakpoint, the TSS-RESTREND method calculates the significance of each identified change. For more details on the TSS-RESTREND method, see Burrell et al. (2017).

In our study, the TSS-RESTREND method was applied using the TSS.RESTREND package for the R software environment (R Core Team, 2017). Some adjustments were required to process raster files and to run the program automatically. Although this method is usually applied to NDVI data (Burrell et al., 2017), in the present work, it was also applied to the other two spectral indices under study (ISA and EVI) through the composite monthly time series (372 months). The OAP was calculated using the CHIRPS precipitation data for accumulation periods of 1-12 months and lag times of 0-3 months, resulting in an increase of 15 months at the beginning of the precipitation series. The decomposition of the time series into seasons used by the BFAST method should not be applied to TSS-RESTREND method because this procedure is previously performed in the RESTREND step.

It is common to limit/exclude pixels that do not follow a pattern from LCC analyses. For instance, Dutrieux et al. (2015) used a mask to process only forested pixels, while Burrell et al. (2017) excluded pixels classified as irrigated agricultural areas from their methodology. These practices are justified either by the specific objectives of the studies or because the techniques are not suitable for that type of land cover (Burrell et al., 2017; Dutrieux et al., 2015). In the Caatinga region, the main economic activities are livestock and subsistence farming. As irrigated crop techniques are not used as much in the study area, we decided to process all of the pixels, regardless of its current land cover.

3.3 Validation Methodology

The performance of the TSS-RESTREND method was evaluated at both temporal and spatial levels and applied to each of the 400 thousand pixels contained in the study area. For each spectral variable (ISA, EVI and NDVI) and pixel, the year of the most significant breakpoint was registered and used to evaluate the spectral variable ability to detect the year (time/period) of the land cover change. The output of the method was compared with the true year of LCC determined by combining the analysis of RapidEye images with visual interpretation of a set of images from Google Earth (http:earth.google.com/).

The validation dataset used in this work was built using a two-step procedure. First, a detailed visual survey of recent (2015) RapidEye images allowed the identification of several target areas where the original land cover had changed by the complete removal of the vegetation (land-cover clearing). In this fragile biome, the "clearing" occurs very often. Most of the time, it is caused by ill-planned land use. Wood removal for firewood/charcoal use is very common in a biome that is almost without conservation units and protected areas. Natural recuperation is too slow. Reforestation initiatives are rare in Caatinga. Therefore, after a "clearing", there is a great possibility for a long-term "land-cover change" to happen (Araujo et al., 2007; Lima et al., 2016). Then, Google Earth imagery was examined to determine the exact date of the land cover change. Additionally, several places that had no visible human impact and that kept their original vegetation cover were also chosen as validation pixels. To confirm the preservation/land-cover clearing state of all these places, field observations were done in October 2017. Two different types of areas were included in the validation dataset (Fig. 3): 1) 35 target areas of 120 m buffer each (ca. 81 pixels), 31 exhibit LCC in the period 1985-2015 and 4 show a preserved natural vegetation; and 2) a small region of 7.5 km^2 (8,300 pixels) that has undergone a well-delimited time-space vegetated/land-cover clearing process over the 2001–2012 period, hereafter referred to as "the polygon".

The mean value of each spectral variable was calculated for each month/year composite image for each one of the 35 selected target areas. The observed year (time/period) of change was compared with the output of the method, and the results were classified into three classes: “Detected true”, when the absolute difference between the year of the detected breakpoint and the true year of change was less than or equal to two years; “Detected false”, when this absolute difference was greater than two years; and “Undetected”, when the TSS-RESTREND method did not detect any significant trend change on the spectral variable time-series, but a LCC process actually occurred. For the four preserved target areas ("No Change"), the result was assigned “Detected true” if no significant breakpoint was detected by the method and “Detected false” otherwise.

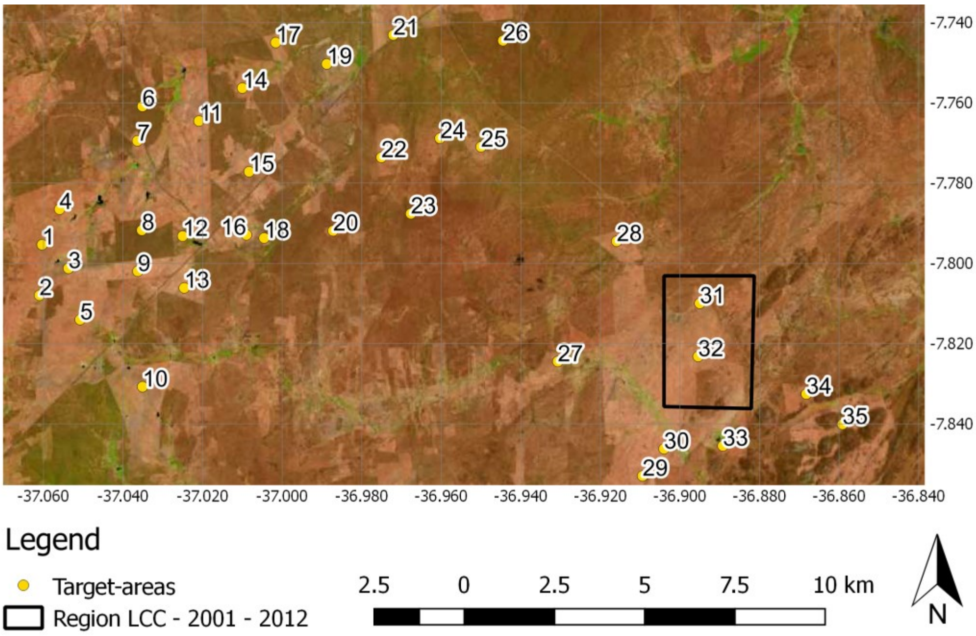

Fig. 3 - Location of the validation dataset in the study area: 35 target areas (numbered) and the polygon that shows a sequential land-cover change process during 2001-2012 (Xmin: -36.90; Xmax: -36.88; Ymin: -7.84; Ymax: -7.80, WGS 84).

The polygon illustrates the process of fragmentation of land-cover clearing and the ability of the proposed methodology to identify these sequential changes. Within this area, pixels exhibiting land clearing in the same year were encompassed within the same patch. To allow a better visual analysis of the detected breakpoint/observed year of changes, these patches were superimposed on both rasters of the TSS-RESTREND output and visible images. In addition, the median was calculated for the output of all pixels within each patch, providing a quantitative comparison between the detected breakpoint and the observed year of change. The median rather than the mean was used as a summary measure because it is a robust statistic of central tendency, not influenced by extreme values (outliers).

4 Results

Our analyses show that the two main differences between the inverse surface albedo (ISA) and the EVI and NDVI are the (i) amplitude of the signal and (ii) the number of breakpoints detected by the TSS-RESTREND method. Whereas values of EVI (NDVI) range between 0.09 and 0.60 (0.1 and to 0.75), ISA values vary only between 0.75 and 0.90. Moreover, the number of the breakpoints detected by using EVI and NDVI is also higher than that with ISA (Fig. 4). Most of the breakpoints occur during a drought period (SPEI < -1, cf. Fig. 2), especially for EVI and NDVI.

In general, despite the lower amplitude and the smaller number of breakpoints detected when using ISA, the TSS-RESTREND method showed the best performance in a land-cover (un)change detection (at a yearly scale) when applied to this spectral variable (Fig. 5). Figure 5B summarizes the efficiency of each index. From the 31 target areas, 25 areas had their land cover cleared. The accuracy rate (81%) of the ISA contrasts with the lower rates achieved with the EVI and NDVI (14% and 29%, respectively). Furthermore, only ISA did not detect any change in the four target areas free from human impact (target areas 6, 8, 23 and 26) (Fig. 5B). Overall, the application of the TSS-RESTREND using the ISA was able to detect drastic human action (clearing) on the Caatinga vegetation and the time of its occurrence (within an interval of two years) in 83% ("Detected true") of the target areas monitored (Table 2), whereas the EVI and NDVI were not able to accurately detect the land cover (un)change in more than 65% of the target areas.

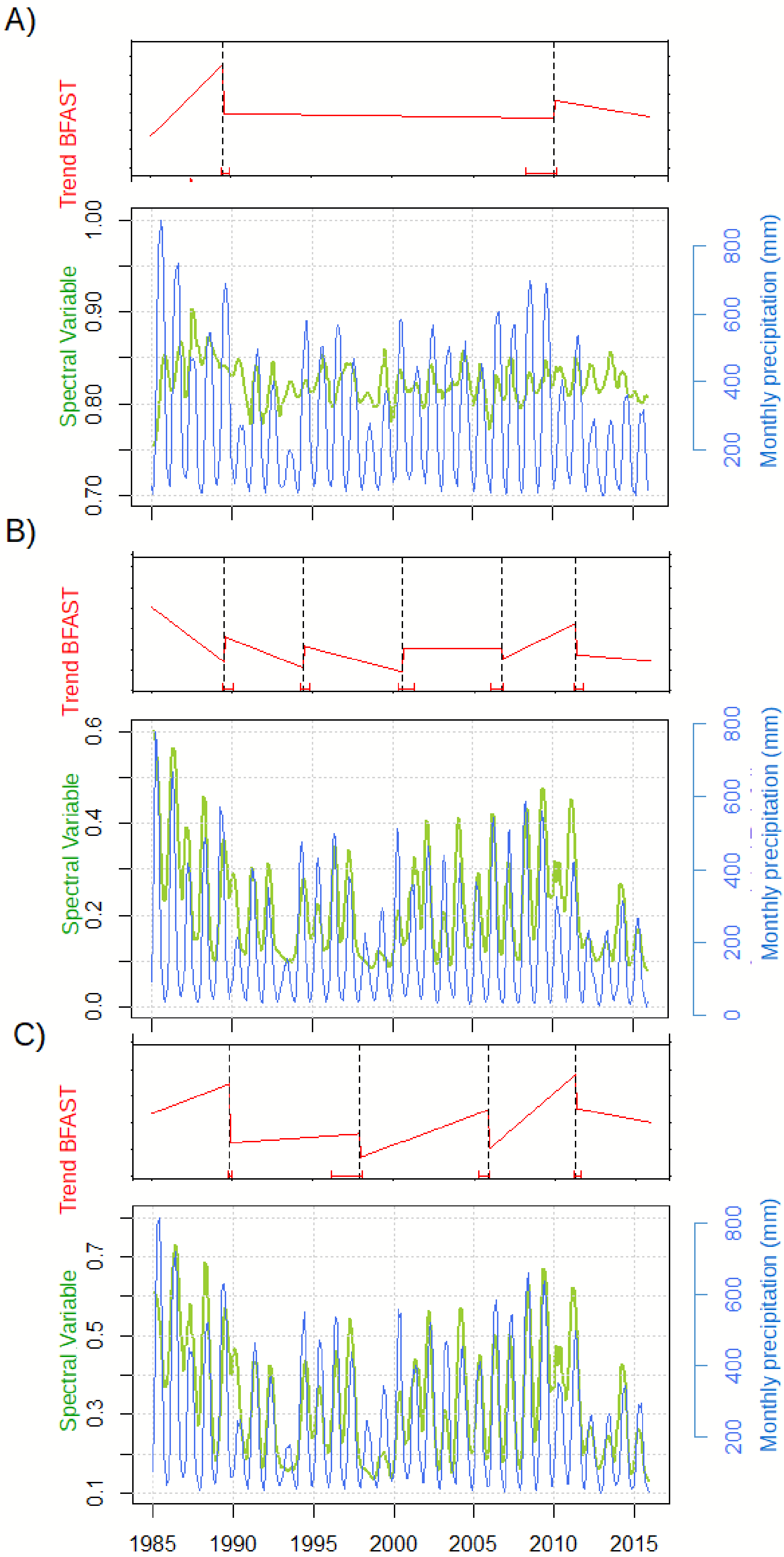

Fig. 4: TSS-RESTREND outputs for the pixel at geographic coordinates x: -37.00445, y: -7.79378; BFAST breakpoint identification, VPR-residuals times series and spectral variables and precipitation times series in (A) ISA, (B) EVI and (C) NDVI.

The very low performance of the TSS-RESTREND method applied to the EVI data was a consequence of the high number of target areas where no significant breakpoint was identified. The land-cover clearing that occurred in 49% of the target areas was not detected by this methodology (TSS-RESTREND and EVI). Although the results obtained with NDVI were better than the ones obtained with EVI (the number of target areas classified as “Detected True” were doubled in comparison), the TSS-RESTREND algorithm implemented with NDVI data incorrectly detected the year of change in 40% of the cases (Table 2).

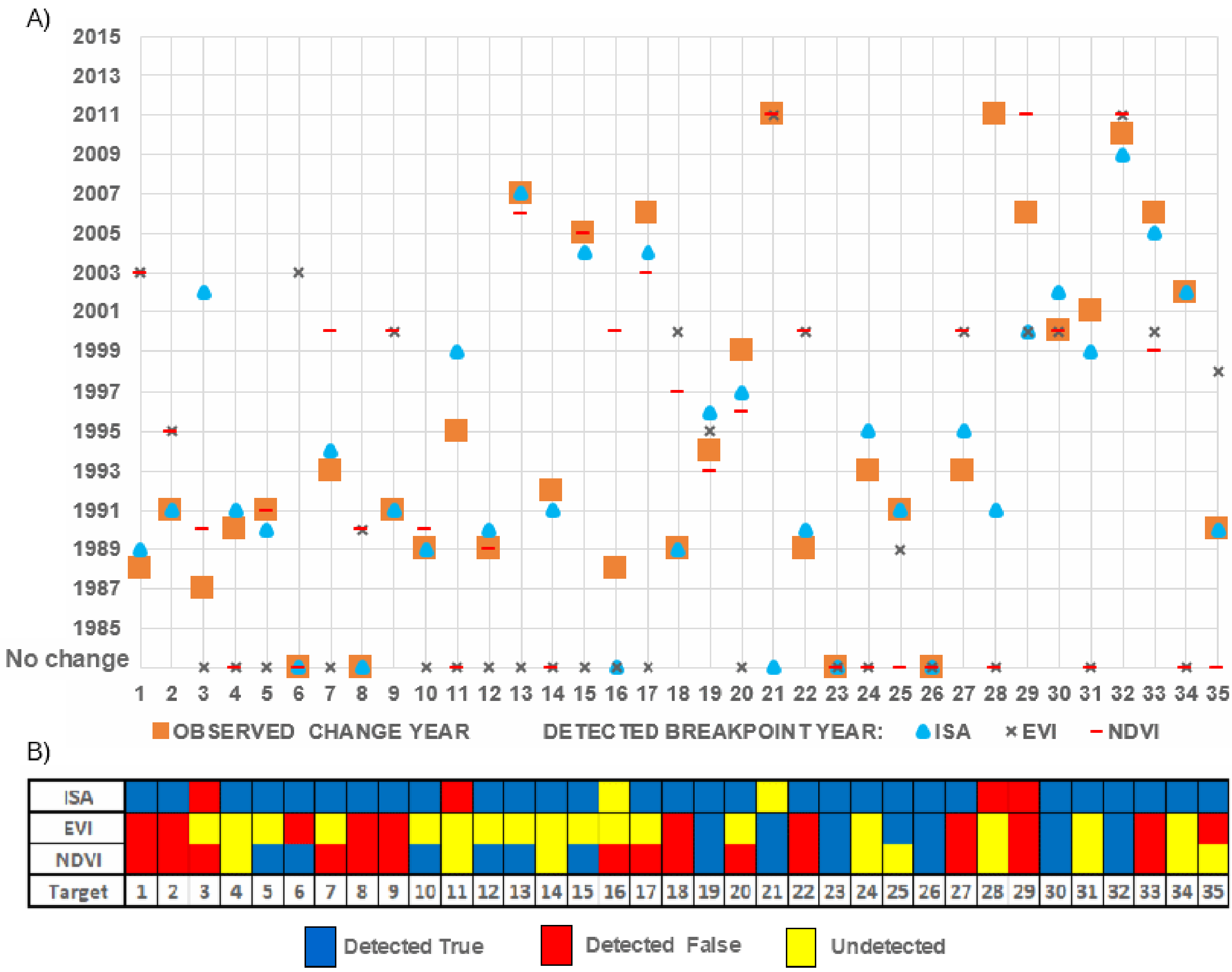

Fig. 5 – Year of change in land cover detected by the TSS-RESTREND method for ISA, EVI and NDVI and observed year of change for the 35 target areas: A) Description and B) Summary

Table 2 – Number of validation target areas in the different classes (and percentage of the total) according to the results of the TSS-RESTREND method applied with the three spectral variables (Fig. 5).

Index	Detected True	Detected False	Undetected
ISA	29 (83%)	4 (11%)	2 (6%)
EVI	7 (20%)	11 (31%)	17 (49%)
NDVI	12 (34%)	14 (40%)	9 (26%)

Two target areas are used within the polygon to validate our results (Fig. 6A). These target areas exhibited contrasting performances: the LCC in target area 31 was only detected by the ISA, while the LCC for target area 32 was correctly detected for all three indices. Within the polygon, the main changes in land cover occurred between 2003 and 2012 (Fig. 7A) and were merged into nine different patches (Figs. 6B and 7A). When EVI and NDVI were used, there were a substantial number of pixels (sometimes > 40%) where no significant breakpoint was found (Fig. 7B). This situation was particularly relevant in the areas where the clearing took place in the years 2003, 2004, 2008 and 2010 (Fig. 6A and 7B). In contrast, the ISA showed that "Undetected" pixels were less than 10% for all the patches (Fig. 7B) and demonstrated an overall better accuracy in identifying the observed LCC with a R^2 of 0.91 (Fig. 7C). The best performance of the EVI and NDVI was observed for the patches where the clearing of vegetation took place in the years 2011 and 2012 (Figs. 6 and 7). However, for the other years and for a large number of pixels, the detected year of LCC was around the years of a severe drought (1993 and 2000, cf. Fig. 2). To have a better insight of the output of TSS-RESTREND applied with the different indices in the validation polygon, bar plots of the detected breakpoint year for the nine patches are shown in Fig. 8. In these graphs, the inability of the method to detect the observed LCC is clear when applied to the usual spectral vegetation indices, EVI and NDVI. The foremost detected breakpoint years are the drought years of 1990 and 2000 and the period of approximately

2010. Although the variability of the ISA results is much higher than that of EVI and NDVI, the detected year of change is closer to the observed date in the former index. Furthermore, while the validation polygon is hardly identified in the output raster of these two vegetation indices, it is quite well-defined in the ISA raster (Fig. 6). This result is a consequence of the TSS-RESTREND ability to distinguish between unchanged and changed pixels with different indices.

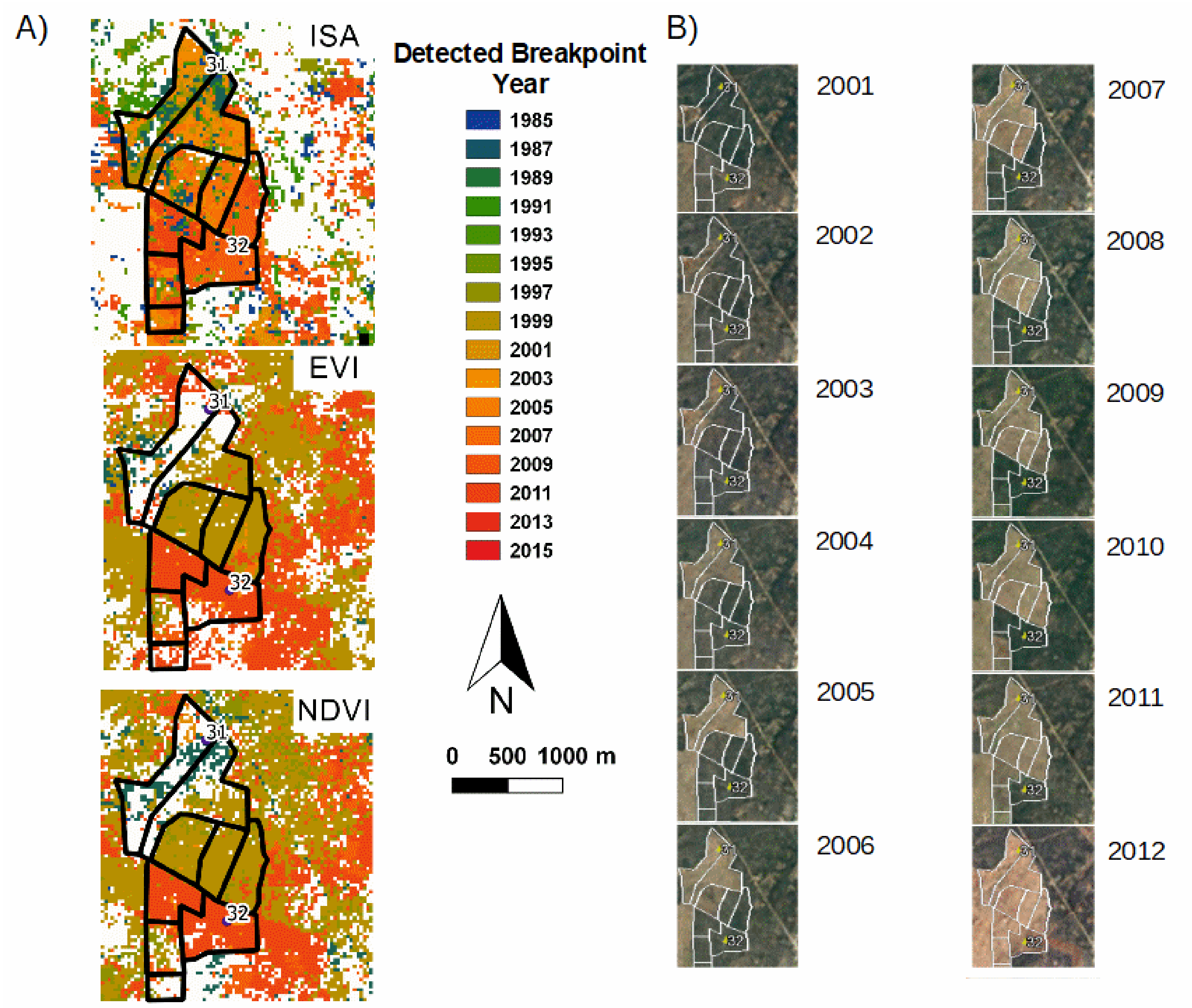

Fig. 6 – Raster-detected breakpoint year of land-cover change (LCC) from TSS-RESTREND for ISA, EVI and NDVI (A) and Google Earth Images and polygon of observed change year of land cover (B).

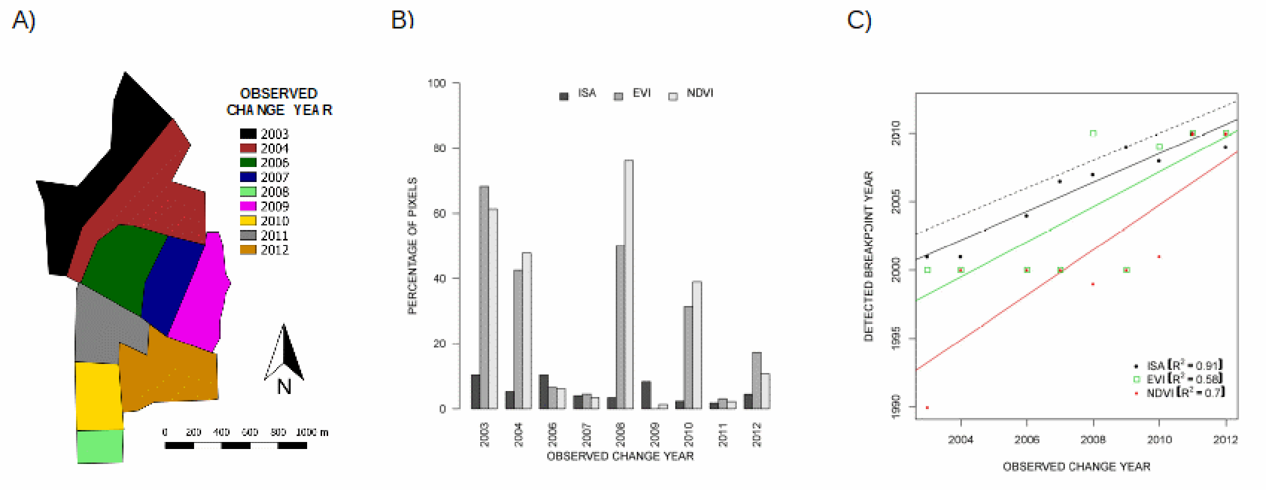

Fig. 7 - Observed change year of land-cover of the different patches compared with the results obtained with the TSS-RESTREND method for the ISA, NDVI and EVI: A) Observed change year of land-cover for each patch; B) percentage of the total number of pixels in each patch where breakpoint was not detected; C) median of the detected breakpoint year for all the pixels where LCC was detected. The dotted line is the 1:1 line, and solid lines are the linear regression for each dataset (with the corresponding coefficient of determination, R^2, shown between brackets).

Visual comparison of this raster with the Google Earth images sequence shows that the TSS-RESTREND methodology applied to ISA has some difficulty in identifying the correct year of clearing when it occurs during the initial and final years of the time series (1985-1990 and 2010-2015, Fig. 9A). The region between target areas 2 and 4 (Fig. 9B) was cleared before 1990, and TSS-RESTREND was not able to identify this change. Likewise, the region immediately above target area 30 suffered a drastic clearing between 1985 and 1990, and, once again, this methodology could not detect it (Fig. 9C). On the other hand, TSS-RESTREND and ISA did a good job spotting the small vegetation patches that remain unchanged during the period of the study (e.g., the regions between target areas 8–9 and 32–33).

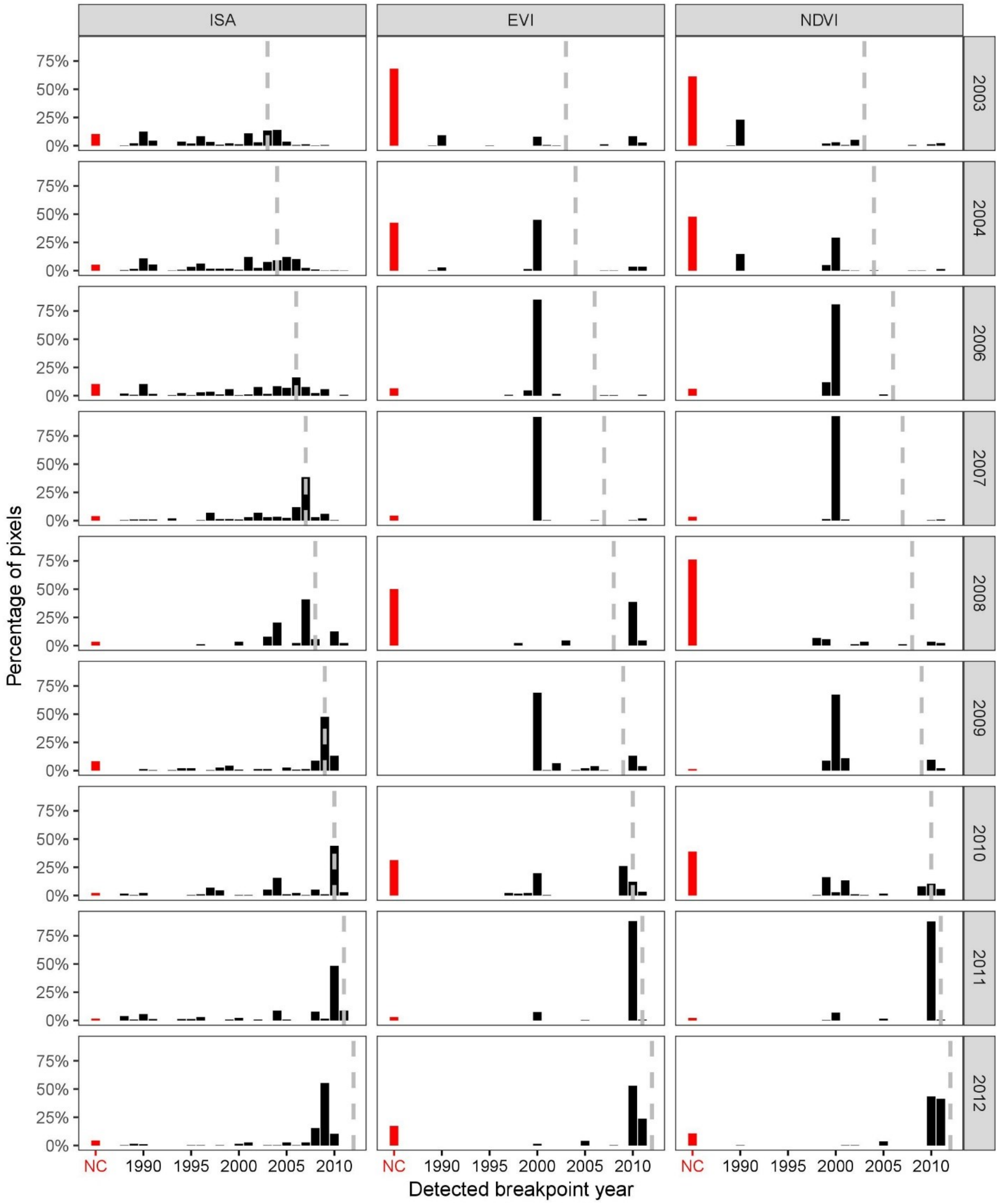

Figure 8 – Bar plots of the detected breakpoint year obtained by the TSS-RESTREND method applied to the three spectral indices (ISA, EVI and NDVI) for the different patches of the validation polygon. Each patch is identified by the year of the observed vegetation clearing (also marked by the grey dashed lines). The height of each black bar is the percentage of pixels where a change was detected in that year. Red bars correspond to pixels where no change was detected.

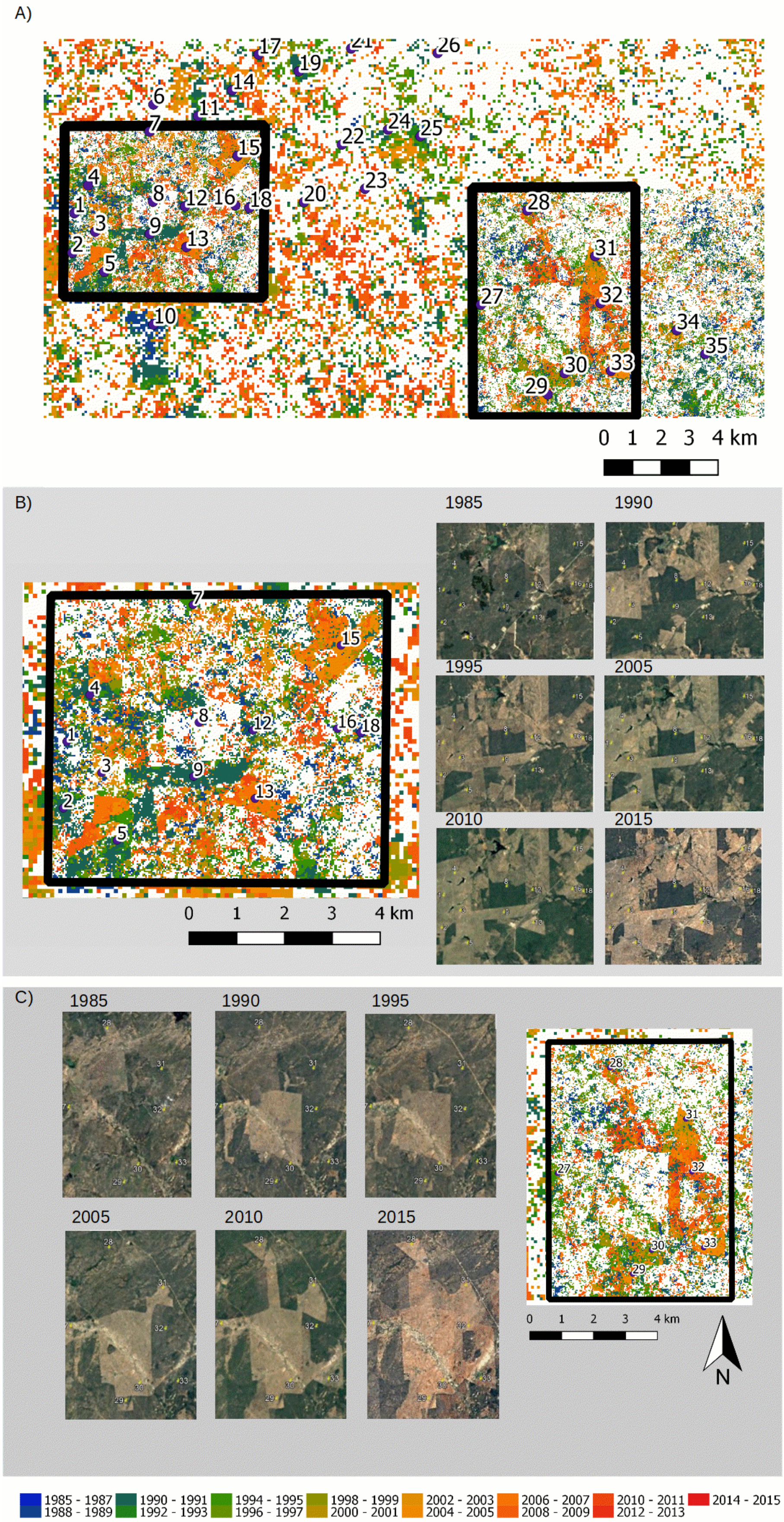

Figure 9 - Detected breakpoint year of LCC from the use of the ISA in the TSS-RESTREND method for the whole study area in (A) and highlights (B and C).

5 Discussion

The use of RapidEye and Google Earth imagery in our analysis allowed us to observe that reforestation or replanting did not occur after land-cover clearing. The areas that have been deforested were mostly occupied by livestock and developed few underbrush or grasses afterwards. Additionally, the low natural fertility condition of the shallow and heterogeneous soils of Caatinga allows only a slow reestablishment of native vegetation upon abandonment (Salcedo et al., 1997; Sobrinho et al, 2016). Therefore, historical LCC in this region is defined by a single moment of clearing in the past decades. To that end, the TSS-RESTREND method was appropriated because it only considers the most significant breakpoint.

Our study suggests that in the Brazilian Caatinga, neither EVI nor NDVI are reliable spectral vegetation indices for identifying land-cover clearing because signals of deciduous vegetation in the leafless period and bare soil are similar to both indices. Despite the wide acceptance of using NDVI (Leroux et al., 2017) and the robustness of EVI to atmospheric aerosols (Huete et al., 2002), with regard to distinguishing the effects of climate variability and anthropic impact on changes in land cover, TSS-RESTREND applied to these indices presented a low performance in detection of the correct timing of the vegetation clearing. Not only is there a very high rate of undetected LCC (cf. Table 2, Figs. 6A and 7B), but also the observed and detected breakpoint years are far from an acceptable standard (cf. Figs. 7C and 8). Most of the detected breakpoints with these indices occurred in the dry years of 1990 and 2000. We ascribe the good performance of EVI and NDVI found in 2010–2012 to a circumstantial combination of the climate conditions in this period. While 2011 was a wet year (maximum SPEI > 2.4), 2012 was the beginning of an extremely dry period, with rainfall amounts well below the total average and drought conditions (SPEI < - 0.5) remaining until 2014 (Fig. 2). When TSS-RESTREND is applied to the NDVI or EVI time series, the phenological changes in Caatinga vegetation due to these severe climate conditions are not distinguished from the LCC driven by human actions.

NDVI was not able to distinguishing anthropic changes from those resulting from climatic variability, even using methods such as TSS-RESTREND that aim to remove the seasonal influence of precipitation. We ascribe the low performance of NDVI under these circumstances to the fact that NDVI values for bare soil and dry grass are not very different (Jones and Vaughan, 2010). As in non-photosynthetic materials (e.g., dry/dead vegetation and bare soil) the reflectance difference between red and NIR is stable; most vegetation indices, defined on these two bands, cannot detect differences in these land cover types (Xu et al., 2014). In contrast, SA allows the monitoring of the target in other bands (visible, NIR and SWIR) of the electromagnetic spectrum, which are not used in EVI and NDVI. This feature gives SA a greater sensitivity to changes involving more characteristics than just the greenness of leaves. When a soil-plant-atmosphere system is altered by an action of deforestation, wood and other plant debris are removed in addition to the loss of leaves, and soil is completely exposed to the effects of radiation, rain and wind that together will modify the state of the soil. This set of modifications can be better detected by the surface albedo than by NDVI and EVI.

Since soil moisture has a high influence on SA, the spectral signals of dry and wet bare soil can be quite different (Fimbres, 2017), and the variation of SA values should be interpreted with caution when addressing LCC analysis. The soils of our study area are shallow and present a low water storage capacity. When the land cover is cleared, the root zone storage is reduced, and as a result, SA increases. In soils with greater depth and water retention capacities, SA may present lower performance as an indicator of alteration in the land cover, which is not the case for most of the Caatinga. Spectral variables that use NIR and SWIR bands also show a better ability to detect plant phenology than that of NDVI and EVI (Jin et al., 2013) by being more sensitive to the water content of vegetation and soil.

DeVries et al. (2015) identified that the indices using the short wave infrared (SWIR) spectral bands are more sensitive to LCC, especially the Tasseled Cap Wetness (TCW) index. The TCW index is defined on the same spectral bands used to calculate SA, which corroborates our results. The spectral band SWIR provides a robust way to estimate the extent of bare soil and vegetation cover in arid and semi-arid regions (Asner and Lobell, 2000). The soil moisture factor may have been responsible for two of the errors detected when using ISA. Target areas 3 and 28 are located near reservoirs and had their breakpoints detected in years of severe drought when the reservoirs were completely dry.

When using the ISA, the TSS-RESTREND showed a high accuracy in the detection of land-cover clearing (83%), but with a gap of ± 2 years. This imprecision should be related to the characteristics of ISA. On the one hand, after vegetation removal, the remaining plant ecosystem (i.e., underground roots and soil) requires time to adapt to the new conditions, which will cause loss of moisture and delay the SA signal response as well as the breakpoint. On the other hand, there is some imprecision of the TSS-RESTREND when the vegetation clearing occurs near very dry years (before or after), which traps the breakpoint into a moment of this period. For example, most of the LCC observed in 2005 and 2006 (target areas 15, 17 and 33) was detected in the year 2003, which was a very dry antecedent year. In the target areas 11 and 29, this gap was greater than the typical 2-year gap, shifting the detected breakpoint year due to drought closer to the land-cover clearing year.

When we used NDVI and EVI, it was not possible to observe a temporal pattern for the low performance in the detection of land-cover clearing by the TSS-RESTREND. The undetected LCC in two areas by the ISA represented areas that had their vegetation removed in either the first or last five years of the time series. In these intervals (1985–1990 and 2010–2015), when using ISA, the TSS-RESTREND method shows limitations in establishing a breakpoint. One possible explanation for the difficulty of TSS-RESTREND in detecting a breakpoint in the first/last years of an ISA time series can be the problem of performing a statistical hypothesis test (the Chow test) with a small sample (say, the first/last five data points) of a variable (ISA) that has a narrow range of values. When the information (sample) is small, the null hypothesis of the test (corresponding to a non-significant breakpoint) will hardly be rejected at the usual significance levels. Under these circumstances, TSS-RESTREND will not detect any land cover change. This situation is particularly evident in the initial years as shown in Fig. 9.

Our study supports further research towards a better understanding of Caatinga land-cover dynamics. Based on this study, further analysis and developments should take place as (i) a deep analysis of SA applications in LCC studies in seasonal tropical dry forests; (ii) a cross-related analysis of SA and other variables, such as evapotranspiration and soil moisture, provided by remote sensing data; and (iii) conservation studies focused on protection and reforestation initiatives.

6 Conclusion

The spatial resolution and long-term series of the Landsat images allowed a high-standard assessment of altered targets in the surface, arranged due to the fragmented nature of the LCC in the studied area. By using this dataset, the application of the TSS-RESTREND method was effective and showed that the ISA exhibited the best performance in identifying the year of land-cover clearing.

TSS-RESTREND showed a satisfactory performance in using long-term satellite data to identify breakpoints of LCC in the Caatinga. The concept of this method is compatible with the reality of the LCC dynamics in this biome, since the selection of the more significant breakpoint unveils the land cover clearing without subsequent vegetation reestablishment. We found some imprecision in the method to identify LCC with a higher frequency of undetected breakpoints in the extreme part of the series (i.e., 1985–1990 and 2010–2015), which were not significant due to the long time series used in this study.

For all situations, the surface albedo presented better performance than that of NDVI and EVI. The ISA was able to distinguish LCC with high accuracy. The lower performance in the application of the TSS-RESTREND method when using the EVI and NDVI indices in the detection of LCC in the Caatinga biome is explained by its high sensitivity to leaf cover variations as a result of seasonal or extreme dry conditions. Changes in land cover affect the entire soil-plant-atmosphere system, such as removal of biomass and changes in soil properties, as well as in the microclimate, due to direct exposure to radiation, precipitation and wind. Based on those changes, studies should not only rely on greenness indices but also look for spectral ranges that will better represent the peculiar characteristics of lesser-known ecosystems.

7 Acknowledgments

This work has been funded by the Brazilian National Council for Scientific and Technological Development (grant numbers 490115/2013-6 and 310789/2016-8) and the European Commission (grant number FP7-614048) through the EUBrazilCC project (http://eubrazilcloudconnect.eu/), CAPES-ANA (grant number 88887.115880/2015-01), and CAPES/PDSE (grant number 88881.134740/2016-01). The Forest Research Centre (CEF) is a research unit funded by Fundação para a Ciência e a Tecnologia I.P. (FCT), Portugal (UID/AGR/00239/2013).

8 Reference

Albuquerque, U.P., de Lima Araújo, E., El-Deir, A.C.A., de Lima, A.L.A., Souto, A., Bezerra, B.M., Ferraz, E.M.N., Maria Xavier Freire, E., Sampaio, E.V. de S.B., Las-Casas, F.M.G., de Moura, G.J.B., Pereira, G.A., de Melo, J.G., Alves Ramos, M., Rodal, M.J.N., Schiel, N., de Lyra-Neves, R.M., Alves, R.R.N., de Azevedo-Júnior, S.M., Telino Júnior, W.R., Severi, W., 2012. Caatinga Revisited: Ecology and Conservation of an Important Seasonal Dry Forest, The Scientific World Journal. doi:10.1100/2012/205182

Alley, W.M., 1988. Using exogenous variables in testing for monotonic trends in hydrologic time series. Water Resour. Res. 24, 1955–1961. doi:10.1029/WR024i011p01955

Alvares, C.A., Stape, J.L., Sentelhas, P.C., De Moraes Gonçalves, J.L., Sparovek, G., 2013. Köppen's climate classification map for Brazil. Meteorol. Zeitschrift 22, 711–728.

doi:10.1127/0941-2948/2013/0507

Andrade-Silva, A.C.R., Nemésio, A., de Oliveira, F.F., Nascimento, F.S., 2012. Spatial-Temporal Variation in Orchid Bee Communities (Hymenoptera: Apidae) in Remnants of Arboreal Caatinga in the Chapada Diamantina Region, State of Bahia, Brazil. Neotrop. Entomol. 41, 296–305. doi:10.1007/s13744-012-0053-9

Anyamba, A., Small, J.L., Tucker, C.J., Pak, E.W., 2014. Thirty-two Years of Sahelian Zone Growing Season Non-Stationary NDVI3g Patterns. Remote Sens. 6, 3101–3122. doi:10.3390/rs6043101

Araújo, E.L., Castro, C.C., Albuquerque, U.P., 2007. Dynamics of Brazilian Caatinga – A Review Concerning the Plants , Environment and People. Funct. Ecosyst. Communities 1, 15–28.

Araújo, V.F.P., Bandeira, a G., Vasconcellos, a, 2010. Abundance and stratification of soil macroarthropods in a Caatinga Forest in Northeast Brazil. Braz. J. Biol. 70, 737–46. doi:10.1590/S1519-69842010000400006

Asner, G.P., Lobell, D.B., 2000. A Biogeophysical Approach for Automated SWIR Unmixing of Soils and Vegetation 4257.

Balzarolo, M., Vicca, S., Nguy-Robertson, A.L., Bonal, D., Elbers, J.A., Fu, Y.H., Grünwald, T., Horemans, J.A., Papale, D., Peñuelas, J., Suyker, A., Veroustraete, F., 2016. Matching the phenology of Net Ecosystem Exchange and vegetation indices estimated with MODIS and FLUXNET in-situ observations. Remote Sens. Environ. 174, 290–300. doi:10.1016/j.rse.2015.12.017

Begueria, S., Latorre, B., Reig, F., Vicente-Serrano, S.M. 2017. Global SPEI database. http://spei.csic.es/database.html. Access in 11 January 2017.

Belchior, M., Tai, D.W., Held, F.C. Von, 2017. Indicadores IBGE. Inst. Bras. Geogr. E Estatística - Ibge 6.

Brito, A.F., Presley, S.J., Santos, G.M.M., 2012. Temporal and trophic niche overlap in a guild of flower-visiting ants in a seasonal semi-arid tropical environment, Journal of Arid Environments. doi:10.1016/j.jaridenv.2012.07.001

Burrell, A.L., Evans, J.P., Liu, Y., 2017. Detecting dryland degradation using Time Series Segmentation and Residual Trend analysis (TSS-RESTREND). Remote Sens. Environ. doi:10.1016/j.rse.2017.05.018

Cai, H., Wang, J., Feng, Y., Wang, M., Qin, Z., Dunn, J.B., 2016. Consideration of land use change-induced surface albedo effects in life-cycle analysis of biofuels. Energy Environ. Sci. 9, 2855–2867. doi:http://dx.doi.org/10.1039/C6EE01728B

Chen, J., Jönsson, P., Tamura, M., Gu, Z., Matsushita, B., Eklundh, L., 2004. A simple method for reconstructing a high-quality NDVI time-series data set based on the Savitzky-Golay filter. Remote Sens. Environ. 91, 332–344. doi:10.1016/j.rse.2004.03.014

Chow, G.C., 1960. Tests of equality between sets of coefficients in two linear regressions. Econometrica 28:591–605. http://dx.doi.org/10.2307/1910133.

De Jong, R., Verbesselt, J., Schaepman, M.E., de Bruin, S., 2012. Trend changes in global greening and browning: Contribution of short-term trends to longer-term change. Glob. Chang. Biol. doi:10.1111/j.1365-2486.2011.02578.x

DeVries, B., Verbesselt, J., Kooistra, L., Herold, M., 2015. Robust monitoring of small-scale forest disturbances in a tropical montane forest using Landsat time series. Remote Sens. Environ. doi:10.1016/j.rse.2015.02.012

Dutrieux, L.P., Verbesselt, J., Kooistra, L., Herold, M., 2015. Monitoring forest cover loss using multiple data streams, a case study of a tropical dry forest in Bolivia. ISPRS J. Photogramm. Remote Sens. doi:10.1016/j.isprsjprs.2015.03.015

Erasmi, S., Schucknecht, A., Barbosa, M.P., Matschullat, J., 2014. Vegetation greenness in northeastern brazil and its relation to ENSO warm events. Remote Sens. 6, 3041–3058. doi:10.3390/rs6043041

Evans, J., Geerken, R., 2004. Discrimination between climate and human-induced dryland degradation. J. Arid Environ. 57, 535–554. doi:10.1016/S0140-1963(03)00121-6

Fimbres, A., 2017. Soil Albedo in Relation to Soil Color , Moisture and Roughness . in the Graduate College.

Flood, N., 2013. Seasonal composite Landsat TM/ETM+ Images using the medoid (a multi-dimensional median). Remote Sens. 5, 6481–6500. doi:10.3390/rs5126481

Funk, C., Peterson, P., Landsfeld, M., Pedreros, D., Verdin, J., Shukla, S., Husak, G., Rowland, J., Harrison, L., Hoell, A., Michaelsen, J., 2015. The climate hazards infrared precipitation with stations—a new environmental record for monitoring extremes. Sci. Data 2, 150066. doi:10.1038/sdata.2015.66

Hein, L., De Ridder, N., Hiernaux, P., Leemans, R., De Wit, A., Schaepman, M., 2011. Desertification in the Sahel: Towards better accounting for ecosystem dynamics in the interpretation of remote sensing images. J. Arid Environ. 75, 1164–1172. doi:10.1016/j.jaridenv.2011.05.002

Helsel, D.R., Hirsch, R.M., 2002. Trend Analysis. Stat. Methods Water Resour. Tech. Water Resour. Investig. B. 4, chapter A3 323–355.

Higginbottom, T.P., Symeonakis, E., 2014. Assessing land degradation and desertification using vegetation index data: Current frameworks and future directions. Remote Sens. 6, 9552–9575. doi:10.3390/rs6109552

HOLBEN, B.N., 1986. Characteristics of maximum-value composite images from temporal AVHRR data. Int. J. Remote Sens. 7, 1417–1434. doi:10.1080/01431168608948945

Huete, A., Didan, K., Miura, T., Rodriguez, E.P., Gao, X., Ferreira, L.G., 2002. Overview of the radiometric and biophysical performance of the MODIS vegetation indices. Remote Sens. Environ. 83, 195–213. doi:10.1016/S0034-4257(02)00096-2

Huete, A.R., Liu, H.Q., Batchily, K., J., L. van W., 1997. A comparsion of vegetation indices over a Global set of TM images for EO -MODIS. Remote Sens. Environ. 59, 440–451.

Ibrahim, Y.Z., Balzter, H., Kaduk, J., Tucker, C.J., 2015. Land degradation assessment using residual trend analysis of GIMMS NDVI3g, soil moisture and rainfall in Sub-Saharan West Africa from 1982 to 2012. Remote Sens. 7, 5471–5494. doi:10.3390/rs70505471

Jin, C., Xiao, X., Merbold, L., Arneth, A., Veenendaal, E., Kutsch, W.L., 2013. Phenology and gross primary production of two dominant savanna woodland ecosystems in Southern Africa. Remote Sens. Environ. 135, 189–201. doi:10.1016/j.rse.2013.03.033

Jones H., Vaughan R. (2010).Remote sensing of vegetation. Priciples, techniques, and applications. Use of spectral information for sensing vegetation properties and for image classification. OXFORD University Press, ISBN: 978-0-19-920779-4.

Ju, J., Masek, J.G., 2016. The vegetation greenness trend in Canada and US Alaska from 1984-2012 Landsat data. Remote Sens. Environ. doi:10.1016/j.rse.2016.01.001

Karlson, M., Ostwald, M., 2016. Remote sensing of vegetation in the Sudano-Sahelian zone: A literature review from 1975 to 2014. J. Arid Environ. doi:10.1016/j.jaridenv.2015.08.022

Katsanos, D., Retalis, A., Michaelides, S., 2016. Validation of a high-resolution precipitation database (CHIRPS) over Cyprus for a 30-year period. Atmos. Res. 169, 459–464. doi:10.1016/j.atmosres.2015.05.015

Lambin, E.F., Geist, H.J., Lepers, E., 2003. Dynamics of land use and land cover change in tropical regions. Annu. Rev. Environ. Resour. 28, 205–241. doi:10.1146/annurev.energy.28.050302.105459

Leal, I.R., Da Silva, J.M.C., Tabarelli, M., Lacher, T.E., 2005. Changing the Course of Biodiversity Conservation in the Caatinga of Northeastern Brazil\rCambiando el Curso de la Conservación de Biodiversidad en la Caatinga del Noreste de Brasil. Conserv. Biol. 19, 701–706. doi:10.1111/j.1523-1739.2005.00703.x

Leroux, L., Bégué, A., Lo Seen, D., Jolivot, A., Kayitakire, F., 2017. Driving forces of recent vegetation changes in the Sahel: Lessons learned from regional and local level analyses. Remote Sens. Environ. 191, 38–54. doi:10.1016/j.rse.2017.01.014

Li, X.B., Li, R.H., Li, G.Q., Wang, H., Li, Z.F., Li, X., Hou, X.Y., 2016. Human-induced vegetation degradation and response of soil nitrogen storage in typical steppes in Inner Mongolia, China. J. Arid Environ. doi:10.1016/j.jaridenv.2015.07.013

Lima, A.L.A., Rodal, M.J.N., 2010. Phenology and wood density of plants growing in the semi-arid region of northeastern Brazil, Journal of Arid Environments. doi:10.1016/j.jaridenv.2010.05.009

Lima, G.D.S., Lima, J.R. de F., Silva, N. da, Oliveira, R.S. De, Lucena, R.F.P., 2016. Inventory in situ of plant resources used as fuel in the Semiarid Region of Northeast Brazil. Brazilian J. Biol. Sci. 3, 45. doi:10.21472/bjbs.030505

Linares-palomino, R., Oliveira-filho, A.T., Pennington, R.T., 2011. Seasonally Dry Tropical Forests 3–21. doi:10.5822/978-1-61091-021-7

Lindquist, M.J., 2004. Capital-skill complementarity and inequality over the business cycle. Rev. Econ. Dyn. 7, 519–540. doi:10.1016/j.red.2003.11.001

Loveland, T.R., Dwyer, J.L., 2012. Landsat: Building a strong future. Remote Sens. Environ. 122, 22–29. doi:10.1016/j.rse.2011.09.022

Masek, J.G., Vermote, E.F., Saleous, N.E., Wolfe, R., Hall, F.G., Huemmrich, K.F., Gao, F., Kutler, J., Lim, T., 2006. A Landsat Surface Reflectance Dataset 3, 68–72.

MMA, Brazilian Ministry of the Environment, 2018. http://geocatalogo.mma.gov.br/

Moro, M.F., Lughadha, E.N., Araújo, F.S. De, Martins, F.R., 2016. A Phytogeographical Metaanalysis of the Semiarid Caatinga Domain in Brazil. Bot. Rev. doi:10.1007/s12229-016-9164-z

Queiroz, L. P. 2006. Neotropical savannas and seasonally dry forests: plant diversity, biogeography, and conservation. Chapter 6 - The Brazilian Caatinga:

phytogeographical patterns inferred from distribution data of the Leguminosae. 121-158. ISBN: 0-8493-2987-6

R Core Team, 2017. R: A language and environment for statistical computing. R Foundation for Statistical Computing, Vienna, Austria. URL https://www.R-project.org/.

Rodal, M., Barbosa, M., Thomas, W., 2008. Do the seasonal forests in northeastern Brazil represent a single floristic unit? Brazilian J. Biol. 68, 467–475. doi:10.1590/S1519-69842008000300003

Salcedo, I.H., Tiessen, H., Sampaio, E.V.S.B., 1997. Nutrient availability in, soil samples from shifting cultivation sites in the semi-arid Caatinga of NE Brazil. Agric. Ecosyst. Environ. 65, 177–186. doi:10.1016/S0167-8809(97)00073-X

Santos, a M., Tabarelli, M., 2002. Distance from roads and cities as a predictor of habitat loss and fragmentation in the caatinga vegetation of Brazil. Braz. J. Biol. 62, 897–905. doi:10.1590/S1519-69842002000500020

Santos, R.M., Oliveira-Filho, A.T., Eisenlohr, P. V., Queiroz, L.P., Cardoso, D.B.O.S., Rodal, M.J.N., 2012. Identity and relationships of the Arboreal Caatinga among other floristic units of seasonally dry tropical forests (SDTFs) of north-eastern and Central Brazil, Ecology and Evolution. doi:10.1002/ece3.91

Savitzky, A., Golay, M.J.E., 1964. Smoothing and Differentiation of Data by Simplified Least Squares Procedures. Anal. Chem. 36, 1627–1639. doi:10.1021/ac60214a047

Sobrinho, M. S., Tabarelli, M. , Machado, I. C., Sfair, J. C., Bruna, E. M. and Lopes, A. V. 2016. Land use, fallow period and the recovery of a Caatinga forest. Biotropica, 48: 586-597. doi:10.1111/btp.12334

Schertz, T., Alexander, R., Ohe, D., 1991. The computer program Estimate Trend (ESTREND), a system for the Detection of Trends in Water-quality data 1–63.

Schucknecht, A., Erasmi, S., Niemeyer, I., Matschullat, J., 2013. Assessing vegetation variability and trends in north-eastern Brazil using AVHRR and MODIS NDVI time series. Eur. J. Remote Sens. 46, 40–59. doi:10.5721/EuJRS20134603

Shuai, Y., Masek, J.G., Gao, F., Schaaf, C.B., 2011. An algorithm for the retrieval of 30-m snow-free albedo from Landsat surface reflectance and MODIS BRDF. Remote Sens. Environ. 115, 2204–2216. doi:10.1016/j.rse.2011.04.019

Shuai, Y., Masek, J.G., Gao, F., Schaaf, C.B., He, T., 2014. An approach for the long-term 30-m land surface snow-free albedo retrieval from historic Landsat surface reflectance and MODIS-based a priori anisotropy knowledge. Remote Sens. Environ. 152, 467–479. doi:10.1016/j.rse.2014.07.009

Stroppiana, D., Bordogna, G., Carrara, P., Boschetti, M., Boschetti, L., Brivio, P.A., 2012. A method for extracting burned areas from Landsat TM/ETM+ images by soft aggregation of multiple Spectral Indices and a region growing algorithm. ISPRS J. Photogramm. Remote Sens. 69, 88–102. doi:10.1016/j.isprsjprs.2012.03.001

Tucker, C.J., 1979. Red and photographic infrared linear combinations for monitoring vegetation. Remote Sens. Environ. 8, 127–150. doi:10.1016/0034-4257(79)90013-0

Verbesselt, J., Hyndman, R., Newnham, G., Culvenor, D., 2010. Detecting trend and seasonal changes in satellite image time series. Remote Sens. Environ. doi:10.1016/j.rse.2009.08.014

Verbesselt, J., Umlauf, N., Hirota, M., Holmgren, M., Van Nes, E.H., Herold, M., Zeileis, A., Scheffer, M., 2016. Remotely sensed resilience of tropical forests. Nat. Clim. Chang. doi:10.1038/nclimate3108

Verbesselt, J., Zeileis, A., Herold, M., 2012. Near real-time disturbance detection using satellite image time series. Remote Sens. Environ. doi:10.1016/j.rse.2012.02.022

Vermote, E., Justice, C., Claverie, M., Franch, B., 2016. Remote Sensing of Environment Preliminary analysis of the performance of the Landsat 8 / OLI land surface reflectance product. Remote Sens. Environ. doi:10.1016/j.rse.2016.04.008

Vicente-Serrano S.M., Beguería, S. López-Moreno, J.I., 2010. A Multi-scalar drought index sensitive to global warming: The Standardized Precipitation Evapotranspiration Index - SPEI. Journal of Climate 23, 1696-1718. https://doi.org/10.1175/2009JCLI2909.1

Wang, Z., Erb, A.M., Schaaf, C.B., Sun, Q., Liu, Y., Yang, Y., Shuai, Y., Casey, K.A., Román, M.O., 2016. Remote Sensing of Environment Early spring post- fi re snow albedo dynamics in high latitude boreal forests using Landsat-8 OLI data. Remote Sens. Environ. 185, 71–83. doi:http://dx.doi.org/10.1016/j.rse.2016.02.059

Wang, Z., Schaaf, C.B., Sun, Q., Kim, J., Erb, A.M., Gao, F., Román, M.O., Yang, Y., Petroy, S., Taylor, J.R., Masek, J.G., Morisette, J.T., Zhang, X., Papuga, S.A., 2017. Monitoring land surface albedo and vegetation dynamics using high spatial and temporal resolution synthetic time series from Landsat and the MODIS BRDF/NBAR/albedo product. Int. J. Appl. Earth Obs. Geoinf. doi:10.1016/j.jag.2017.03.008

Wessels, K.J., Prince, S.D., Malherbe, J., Small, J., Frost, P.E., VanZyl, D., 2007. Can human-induced land degradation be distinguished from the effects of rainfall variability? A case study in South Africa. J. Arid Environ. 68, 271–297. doi:10.1016/j.jaridenv.2006.05.015

Wessels, K.J., van den Bergh, F., Scholes, R.J., 2012. Limits to detectability of land degradation by trend analysis of vegetation index data. Remote Sens. Environ. 125, 10–22. doi:10.1016/j.rse.2012.06.022

Wulder, M.A., White, J.C., Loveland, T.R., Woodcock, C.E., Belward, A.S., Cohen, W.B., Fosnight, E.A., Shaw, J., Masek, J.G., Roy, D.P., 2016. The global Landsat archive: Status, consolidation, and direction. Remote Sens. Environ. 185, 271–283. doi:10.1016/j.rse.2015.11.032

Xu, D., Guo, X., Li, Z., Yang, X., Yin, H., 2014. Remote Sensing of Environment Measuring the dead component of mixed grassland with Landsat imagery. Remote Sens. Environ. 142, 33–43. doi:10.1016/j.rse.2013.11.017

Yang, Y., Wang, Z., Li, J., Gang, C., Zhang, Y., Zhang, Y., Odeh, I., Qi, J., 2016. Comparative assessment of grassland degradation dynamics in response to climate variation and human activities in China, Mongolia, Pakistan and Uzbekistan from 2000 to 2013. J. Arid Environ. 135, 164–172. doi:10.1016/j.jaridenv.2016.09.004

Zhang, J., Niu, J.M., Bao, T., Buyantuyev, A., Zhang, Q., Dong, J.J., Zhang, X.F., 2014. Human induced dryland degradation in Ordos Plateau, China, revealed by multilevel statistical modeling of normalized difference vegetation index and rainfall time-series. J. Arid Land 6, 219–229. doi:10.1007/s40333-013-0203-x